ACS Combinatorial Science

Research Article

pubs.acs.org/acscombsci

Utilizing Pulsed Laser Deposition Lateral Inhomogeneity as a Tool in Combinatorial Material Science

David A. Keller,[†] Adam Ginsburg,[†] Hannah-Noa Barad,[†] Klimentiy Shimanovich,[†] Yaniv Bouhadana,[†] Eli Rosh-Hodesh,[†] Ichiro Takeuchi,[§] Hagit Aviv,[†] Yaakov R. Tischler,[†] Assaf Y. Anderson,[†] and Arie Zaban*[,†]

[†]Department of Chemistry, Center for Nanotechnology & Advanced Materials, Bar Ilan University, 5290002 Ramat Gan, Israel

[§]Department of Materials Science and Engineering, University of Maryland, College Park, Maryland 20742, United States

Supporting Information

ABSTRACT: Pulsed laser deposition (PLD) is widely used in combinatorial material science, as it enables rapid fabrication of different composite materials. Nevertheless, this method was usually limited to small substrates, since PLD deposition on large substrate areas results in severe lateral inhomogeneity. A few technical solutions for this problem have been suggested, including the use of different designs of masks, which were meant to prevent inhomogeneity in the thickness, density, and oxidation state of a layer, while only the composition is allowed to be changed. In this study, a possible way to take advantage of the large scale deposition inhomogeneity is demonstrated, choosing an iron oxide PLD-deposited library with continuous compositional spread (CCS) as a model system. An Fe_2O_3−Nb_2O_5 library was fabricated using PLD, without any mask between the targets and the substrate. The library was measured using high-throughput scanners for electrical, structural, and optical properties. A decrease in electrical resistivity that is several orders of magnitude lower than pure α-Fe_2O_3 was achieved at ∼20% Nb−O (measured at 47 and 267 °C) but only at points that are distanced from the center of the PLD plasma plume. Using hierarchical clustering analysis, we show that the PLD inhomogeneity can be used as an additional degree of freedom, helping, in this case, to achieve iron oxide with much lower resistivity.

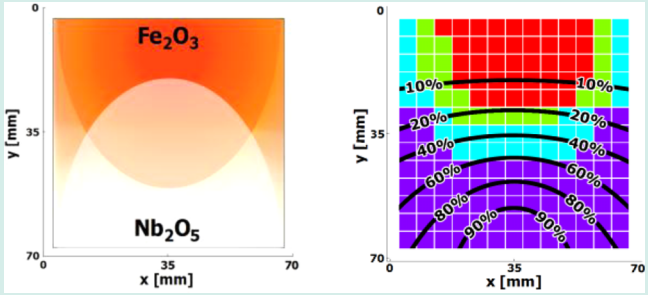

KEYWORDS: *combinatorial material science, pulsed laser deposition (PLD), hematite (α-Fe_2O_3), hierarchical clustering, continuous compositional spread (CCS), thin films, all-oxide photovolatics*

INTRODUCTION

Pulsed laser deposition (PLD) is a major tool in combinatorial material science, as it enables rapid fabrication of different composite materials.[1] This deposition method that is performed in a nonequilibrium manner, is capable of producing submonolayers of material, and is able to form lateral thickness gradients, making it an attractive tool for studying new materials.[2] Complex materials can be grown using sequential PLD deposition of submonolayer amounts of the different constituents, with synchronized substrate and target motions.[3] Nevertheless, this method has typically been limited to small substrates, since PLD deposition on substrate areas larger than the diameter of the plasma plume (∼1 cm), results in severe lateral inhomogeneity.[4] The spatial variation is in regard to the layer thickness, density, and oxidation state, as a function of the distance from the center of the plasma plume.[5] To overcome these shortcomings, a few technical solutions have been suggested, including the use of different designs of masks.[6−9] The use of various masks indeed narrowed the complexity of the deposited films and thus simplified the characterization.

Using PLD, a single sample (also known as a library) with a continuous compositional spread (CCS) was fabricated, creating different ratios between the materials, at different locations in the library.[10] The continuous compositional spread is similar to a phase diagram, where (in the case of oxides) one edge of the library comprises almost pure AO, the other edge comprises almost pure BO, and the points in the middle are different phases of $A_xB_yO_z$ with varying compositions.[11] After the library fabrication, relevant properties are measured throughout the library, using high-throughput characterization systems.[12] However, when no mask is used during the PLD fabrication process, the product library will probably suffer from lateral inhomogeneity with respect to the layer structure, morphology, or oxidation state. Using an iron oxide PLD-based CCS library as a model system, we demonstrate a possible way to handle the inhomogeneity and even to exploit it for our needs. Without the use of masks, an additional degree of

Received: June 19, 2014
Revised: December 23, 2014
Published: March 23, 2015

DOI: 10.1021/co500094h
ACS Comb. Sci. 2015, 17, 209−216

freedom is gained, seemingly serving the combinatorial approach rationale, which is based on many parameters that change within a single experiment.[13]

Metal oxide semiconductors are candidates for various fields of renewable energy, since many metal oxides are chemically stable, nontoxic, and highly abundant.[14] Iron-based oxides are of special interest, mainly because of their high abundance.[15] Hematite (α-Fe_2O_3) is the oldest known iron oxide mineral, and its red-brown color made it an important pigment in the early stages of human history.[16] Hematite is extremely stable and is often the product of the chemical transformation of other iron oxides.[15] Some of the semiconducting properties of α-Fe_2O_3 make it suitable for use in solar harvesting.[17,18] It is an n-type semiconductor with an indirect bandgap of ~2.0−2.2 eV, which allows for absorbance of ~25% of sunlight.[19] However, it has poor electrical properties: high resistivity,[20] short charge carrier diffusion length (a few nm),[21,22] and a short exciton lifetime.[23,24] In addition, its absorption coefficient does not allow for proper light absorption, unless layers with thicknesses much higher than the diffusion length are used. For these reasons, the structure of α-Fe_2O_3, which is used in renewable energy systems, is currently limited to nanoporous layers that allow for sufficient thickness along with a short distance to the charge separation interface.[25−27]

Thus far, to improve the properties of α-Fe_2O_3, many dopants and additives have been examined. The vast majority of past studies focused on low dopant concentrations using discrete and noncontinuous percentages of dopant.[28] We suggest a different method, which may possibly be better, for improving the properties of α-Fe_2O_3, utilizing combinatorial material science.[29] Using PLD-based CCS, a continuous and much wider range of alloying percentages is allowed to be incorporated into Fe_2O_3.

In this study, Nb_2O_5 was selected to be mixed with α-Fe_2O_3. Nb_2O_5 is an n-type, wide-bandgap semiconductor, with a direct bandgap of ~3.4 eV.[30] Nb_2O_5 was mainly chosen because of its high chemical stability and its ionic radius which is similar to α-Fe_2O_3 when both are in their octahedral geometry (Fe^{3+} = 64.5 pm, Nb^{5+} = 64 pm).[31] Because of the discrepancies between the metal ion electrical charges (Fe^{3+}, Nb^{5+}), a very different charge distribution is expected. The different charge distribution can significantly alter the electrical properties of Nb_2O_5-mixed with α-Fe_2O_3 compared to pure α-Fe_2O_3.

Here we present the Fe−Nb−O library results in a broader context of PLD-based CCS libraries. We report a new approach that deals with the lateral inhomogeneity in large-area CCS films deposited by PLD, using the Fe−Nb−O library as a model system. We demonstrate a way to approach the complexity of PLD-based CCS libraries, using hierarchical clustering analysis. We show that what seemed to be a drawback in PLD-based CCS films may even become beneficial,[32] since when using the lateral inhomogeneity approach a major increase in α-Fe_2O_3 conductivity is achieved, depending on both the Nb concentration and on the structural properties of the material, which are independently varied along the library.

EXPERIMENTAL PROCEDURES

Using the combinatorial material science approach, we fabricated a library with a continuous compositional spread of Fe_2O_3−Nb_2O_5 using PLD, which we then measured in high-throughput scanners for optical, electrical, and structural properties. A commercially available, alkali-free, 71 × 71 × 1.1 mm^3, square glass (Corning 7059) was used as a substrate. The Fe−Nb−O layer was deposited by pulsed laser deposition (PLD, Neocera) consisting of a KrF excimer laser with a 248 nm emission wavelength (Coherent, CompexPro102). Deposition was carried out at 600 °C onto a substrate that was preheated via a radiative heater, under an oxygen pressure of 330 mTorr. Two targets were used, an Fe_2O_3 target with a purity of 99.9% and an Nb_2O_5 target with a purity of 99.95% (both Kurt J.Lesker co.), with a target-to-substrate distance of 50 mm. A laser fluence, inside the vacuum chamber, of 90 mJ, and a laser spot size of ~4.1 mm^2, were measured, corresponding to an energy density of ~2 J/cm^2. The laser repetition rate was 8 Hz. Deposition was carried out as layer-by-layer deposition, but the extremely thin layers that are deposited and the temperature cause intermixing between the layers to form a thin film. The Fe_2O_3 target was ablated with 100 laser pulses, followed by a substrate rotation of 180°, and a 20 pulse ablation of the Nb_2O_5 target. The process was repeated for 500 cycles, for a total of 50 000 pulses on the Fe_2O_3 target, and a total of 10 000 pulses on the Nb_2O_5 target. No mask was used between the targets and substrate. The sample was postannealed at 600 °C for 48 h under ambient conditions.

Resistance measurements were performed using a home-built collinear four point probe resistance scanner system. The system consists of a heating sample holder stage, four point probe head with a constant interprobe spacing of 2.5 mm (probes purchased from Ingun Prüfmittelbau GmbH), perspex box for humidity control, Keithley 6517B and Keithley 2400 for a voltmeter and a current supply, respectively. The measurements were performed under a controlled atmosphere (<10% humidity), after the sample was heated to 267 °C for 30 min to desorb water molecules from the surface. At lower temperatures most of the points were too resistive and out of the measuring system range, so measurements were then performed at a high temperature (267 °C) to enable proper mapping of the library. At 267 °C, 103 out of the 169 points of the library were successfully measured, while 66 points were still too resistive for measurement. Resistivity (ρ) was calculated based on the measured resistance (R), using the library thickness and a geometrical correction factor.[33]

Optical transmission (total) and reflection (both specular and total) with a spectral range of 320−1000 nm were measured in ambient conditions, with a home-built scanner. The scanner is an optical fiber based system, consisting of two integrating spheres and a CCD array spectrometer (USB4000, OceanOptics).[32] The measurement points were circular with a diameter of 3 mm. Absorptance was calculated based on the total transmission and total reflection measurements.

Raman spectra were measured with a duel laser Raman system (LabRam HR Raman spectrometer) with the aid of an automated switching filter that allowed for stable and accurate mapping measurements. In each measurement, an excitation laser beam was first transmitted through an objective of 100× to a certain spot on the surface, with a diameter of 2 μm. Then, the scattered light was collected by that same objective into a CCD camera. An excitation wavelength of 532 nm and a measuring range of 50−3000 cm^{-1} were used.

The resistivity, optical and Raman measurements were performed for a grid consisting of 13 × 13 points (169 points total), with a distance of 5 mm between adjacent points. X-ray diffraction measurements were performed with a Rigaku Smartlab workstation, with a θ−2θ scan range of 10−90°.

DOI: 10.1021/co500094h
ACS Comb. Sci. 2015, 17, 209−216

The thickness of the Fe−Nb−O layer was determined using a commercially available optical modeling software (CODE), which fits simulated reflection and transmission spectra, to the measured ones.[34] We used wavelengths ranging from 380 to 1000 nm for the analysis. The simulation was based on the OJL interband transition model[35] and was validated on different samples using SEM images of focused ion beam (FIB) produced cross sections. The SEM micrographs were obtained at the same points using a Helios 600 system (FEI). The thickness profile was based on the optical simulation of both the Fe−Nb−O sample shown here, and two separate samples of Fe_2O_3 and Nb_2O_5 that were deposited under the exact same conditions and were used as references. The sum of both reference simulations was in close agreement with our experimental sample results.

The Energy Dispersive X-ray Spectroscopy (EDS) spectra were obtained by an 80 mm^2 X-max detector (Oxford Instruments), which was mounted on a field emission, FEI, Magellan 400L high-resolution scanning electron microscope (HRSEM).

The composition profile (the Nb_2O_5 atomic fraction) was based on the ratio between the separate thickness profiles of the Fe_2O_3 and the Nb_2O_5 reference samples. The difference in density between the two starting materials was also taken into account. This profile was cross-validated with the EDS spectra, using the ratio of the integrated intensity of the Fe and the Nb related peaks. Both composition profiles were in good agreement with each other.

The hierarchical clustering analysis of the Raman spectra and the optical spectra was performed using CombiView, which is a program that was written in MATLAB for this purpose.[36] This analysis was performed to map out regions within the library that share similar spectral behavior, with regard to the position of the peaks and their relative intensities. The details of this analysis include the choice of a distance function, a linkage method, and a threshold distance.[37] The distance function determines the definition of similarity between two spectra; the linkage method defines the distance between two groups of spectra; and the threshold distance defines the level of similarity within a group and, consequently, the size of the groups. In this case, the Pearson distance function was used. The linkage method was the group complete linkage method, which defines the correlation distance between two groups of spectra, as the largest distance that exists between the spectra within these two groups.[38] The threshold distance was determined such that only four major groups would be formed, as described in the Supporting Information.

RESULTS AND DISCUSSION

A model library of Fe_2O_3−Nb_2O_5 with a continuous compositional spread was fabricated using PLD, without any mask between the targets and the substrate. The library is described schematically in Figure 1a, and an image of the library is given in Figure 1b. The red-brown color in the upper region indicates areas that were closer to the PLD Fe_2O_3 plasma plume, while the transparent region at the bottom indicates areas that were closer to the Nb_2O_5 plume. This PLD deposition pattern yields thickness and composition diversities within the library.

Figure 2a shows the thickness map of the library presented in Figure 1. The two thickness peaks (>300 nm) are positioned at the center of the PLD plasma plume: the upper corresponding to the Fe_2O_3 and the bottom to the Nb_2O_5. A wide range of

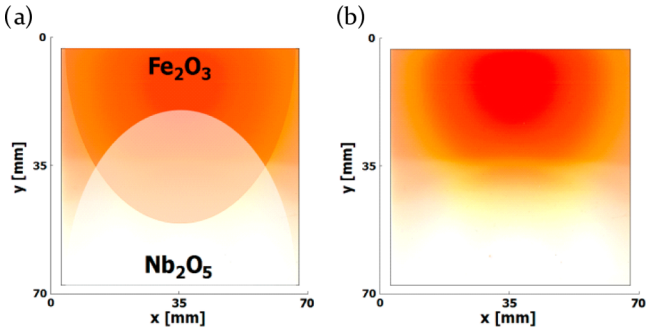

Figure 1. Combinatorial thin film library of Fe−Nb−O: (a) Schematic description of the PLD deposition pattern in the library. (b) Photograph of the library: the red-brown color at the top indicates Fe_2O_3-rich areas; the transparent region at the bottom indicates Nb_2O_5-rich areas.

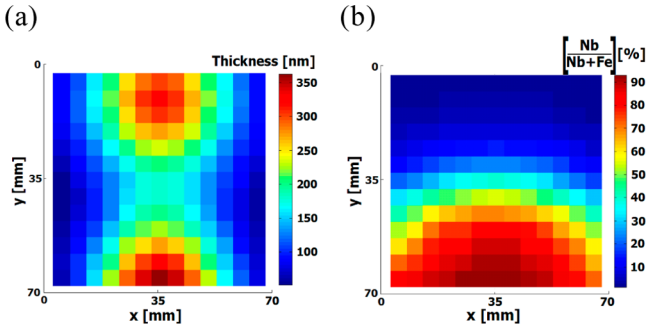

Figure 2. (a) Thickness map of the Fe_2O_3−Nb_2O_5 library showing two peaks (red areas), which are positioned at the center of the PLD plasma plume: Fe_2O_3 (upper) and Nb_2O_5 (lower). (b) Composition map presented by the Nb percent out of the total Fe−Nb content, excluding the Oxygen content. The separated thickness profiles of Fe_2O_3 and Nb_2O_5 reference samples are given in the Supporting Information.

Fe−Nb−O layer thicknesses exists within the library, ranging from 60 to 360 nm.

The library composition map in Figure 2b depicts the percentage of Nb (out of the total Fe−Nb content in the Fe−Nb−O layer) present throughout the library. This is the Nb_2O_5 "doping percentage" or "mixing ratio" in Fe_2O_3 that shows a wide compositional range, with composition ranging between 1% to 92% Nb−O. This range of Nb incorporated into Fe_2O_3 is much wider than that of previous studies, which focused on low doping percentages (<5%). Together with the thickness profile, it is evident that this library contains both a continuous thickness and a compositional spread. There are a vast number of possible combinations of Nb−O percentages and Fe−Nb−O layer thicknesses within the library, allowing for a thorough investigation of the effect of Nb−O incorporation into Fe_2O_3.

Since the electrical behavior of pure α-Fe_2O_3 is the main obstacle preventing its use in renewable energy applications, resistivity (ρ) throughout the library was measured. A large fraction of the library was too resistive to be measured at 47 °C. To circumvent this restriction, the sample temperature was raised to 267 °C to decrease the resistivity in accordance with fundamental semiconductor theory.[39] Even in the higher temperature (267 °C), only 103 of the 169 points in the library were successfully measured, while 66 points were still too resistive for measurement, mainly at points close to pure Fe_2O_3 and Nb_2O_5. Reference samples of pure Fe_2O_3 and

DOI: 10.1021/co500094h
ACS Comb. Sci. 2015, 17, 209−216

Nb_2O_5 were also too resistive for measurement. When resistivity (ρ) is presented as a function of composition (Figure 3), three trends are observed: (1) The lowest resistivity was

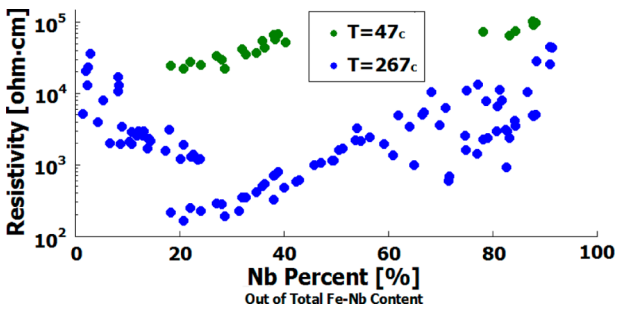

Figure 3. Resistivity [ρ] as a function of the Nb percentage (out of the total Fe−Nb content in the Fe−Nb−O layer), measured at 47 °C [green] and at 267 °C [blue]. A large fraction of the library was too resistive to measure at the former temperature. To circumvent this restriction, the sample temperature was raised to decrease the resistivity in accordance with fundamental semiconductor theory. Even in the high temperature (267 °C), only 103 of the 169 points of the library were successfully measured, while 66 points were still too resistive for measurement, mainly at points with close to pure Fe_2O_3 (far left of the plot) and Nb_2O_5 (far right of the plot). In the blue graph (267 °C), some mixing ratios of Nb show a significant difference in resistivity (more than an order of magnitude) for the same Nb percentages. This phenomenon is especially evident at the two minimum points; with discontinuity at ∼20% Nb and scattered results at ∼70% Nb. The same two minimum points are also observed in lower temperature (47 °C), as can be seen in the green plot.

measured at ∼20% Nb, giving $\sim 10^2$ Ω cm at 267 °C, and $\sim 10^4$ Ω cm at 47 °C. For comparison, pure α-Fe_2O_3 has a resistivity of $\sim 10^{14}$ Ω cm at room temperature.[40] The low resistivity points are located at the periphery of the library, in areas that are far from the center of the PLD plasma plume. A similar trend is observed at a lower temperature (47 °C), as can be seen in the green graph. The significant improvement in the electrical properties of Fe_2O_3 may enable its future use as the main light absorber in all-oxide photovoltaic devices. (2) A local minimum is observed at ∼70% Nb. (3) Some mixing ratios of Nb show a significant difference in resistivity for the same Nb percentages (more than an order of magnitude). This phenomenon is especially evident at the two minimum points mentioned above; with discontinuity at ∼20% Nb and scattered results at ∼70% Nb.

To investigate the properties of the low-resistivity points, as well as the reason for the discontinuous and scattered results, the following high-throughput measurements were performed.

Raman spectra were used to investigate the vibrational modes to infer the structural properties of the library. Because of the complicated nature of the data, which contains 169 spectra and many unidentified peaks, high-throughput analysis was required. The high-throughput analysis can cluster the many spectra into a few subgroups, according to levels of spectral similarity. Using the hierarchical clustering analysis, the 169 Raman spectra were first clustered into subgroups with similar spectra. A similarity threshold was defined (see Supporting Information) to create four groups with similar Raman spectra, as shown in Figure 4a. The four groups were plotted with the same color code on the library map (Figure 4b), to which same-composition (Nb percentage) contours were added.

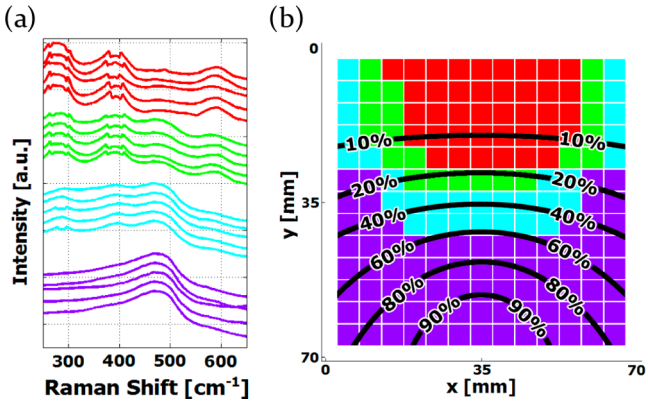

Figure 4. Hierarchical clustering analysis of the Raman data: (a) Five random spectra chosen from each of the four groups, demonstrating similarity between spectra within the same group, and the dissimilarity between spectra from different groups. (b) The four groups of similar Raman spectra marked on the library map by different colors. The composition (Nb percentage) is indicated by black contours. It is clear that some of the points with similar composition have very different Raman spectra.

Despite similar Nb_2O_5 fractions, some of the points show very different spectral behavior. This phenomenon is emphasized at the points containing ∼10−20% Nb, which are found in each of the four different spectral clusters. In other words, despite their similar chemical compositions, different Raman spectra are observed, implying different structures and, therefore, different properties. However, this was not the case for the points containing ∼70% Nb, which were all clustered into one group (purple), having very similar Raman spectra.

It is evident that the physical location of each of the four groups within the library corresponds to the pattern of the α-Fe_2O_3 PLD deposition. Moreover, it seems that the distance from the center of the α-Fe_2O_3 PLD plasma plume is a major factor in the creation of the different clusters, probably due to the different deposition nature in each of the areas. The low resistivity is indeed apparent at the ∼20% Nb points, but only in areas that are close to the edges of the library, at points with Raman spectra that belong to the purple cluster. Not every point with ∼20% Nb shows the lower resistivity, only the ∼20% Nb points that were distanced from the center of the α-Fe_2O_3 PLD plasma plume display low resistivity.

A somewhat similar picture is observed when hierarchical clustering analysis is applied to the UV−vis absorptance spectra. Here also, the 169 spectra were clustered into subgroups according to their level of spectral similarity and a similarity threshold was defined (see Supporting Information). Four groups with similar UV−vis spectra were obtained (Figure 5a) and plotted on the library map (Figure 5b), where composition (Nb_2O_5 percentage) is indicated by black contours. There exists a similarity, although limited, to the Raman hierarchical clustering map in Figure 4b.

We note that the four representative spectra represent variation in the bandgap of the deposited compositions. Consequently, Figure 4a presents a typical direct bandgap Tauc plot for each one of the given groups, showing an increase in the bandgap as the Nb content rises. Full bandgap maps that show a comparable trend were also calculated and are shown in the Supporting Information (Figure S3).

As in the Raman data analysis, the hierarchical clustering analysis of the UV−vis spectra highlights areas that despite

DOI: 10.1021/co500094h
ACS Comb. Sci. 2015, 17, 209−216

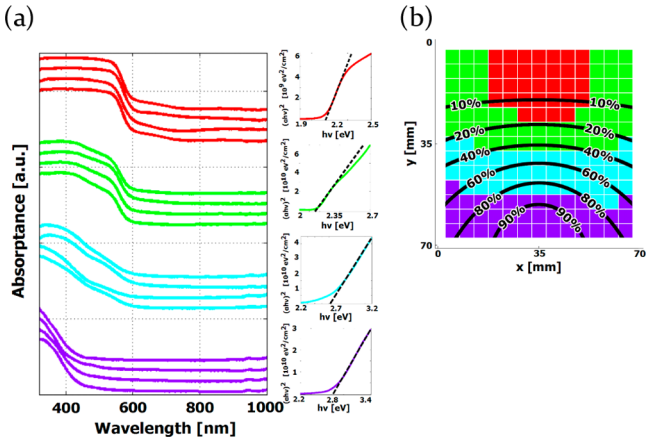

Figure 5. Hierarchical clustering analysis of the UV−vis absorptance data: (a) Four random spectra from each of the four groups, demonstrating the similarity between spectra within the same group, and the dissimilarity between spectra from different groups. A typical Tauc plot (for direct bandgap) for every one of the four groups is shown to the right, displaying a rise in the bandgap as the Nb content increases. Full bandgap maps, which show a similar trend, are presented in the Supporting Information (Figure S3). (b) The groups of similar absorptance spectra marked on the library map by different colors. The composition (Nb percentage) is indicated by black contours. There exists a similarity, although limited, to the Raman hierarchical clustering map in Figure 4b.

having similar chemical compositions, show different and distinct spectral behavior. It seems that the spectral behavior is strongly dependent on the distance from the center of the α-Fe_2O_3 PLD plasma plume, as well as on the chemical composition. Thus, as previously demonstrated,[32] the different physical and structural properties throughout the PLD-deposited library can be seen as an additional degree of freedom, allowing the investigation of not only the different compositions but also the effect of the different PLD deposition natures.

XRD measurements were performed initially along the central vertical line of the library. The XRD patterns of these points are shown in Figure 6a. The physical location of the measured points is shown in Figure 6b. Points with ∼20% and ∼70% Nb are indicated with black contours. In patterns 1, 2, and 3, the only observed crystalline phase was α-Fe_2O_3 hematite. Pattern 7 shows only crystalline Nb_2O_5. Patterns 4, 5, and 6 show inconclusive results, with a small number of peaks that can be related to α-Fe_2O_3, Nb_2O_5, $FeNbO_4$ or many other phases. No conclusive crystalline phase is recognized as the cause for lower resistivity at Nb concentrations of ∼20% and ∼70%. Pattern 3, taken at the ∼20% point, shows the presence of only α-Fe_2O_3 while patterns 1 and 2, each with much higher resistivity, also have only α-Fe_2O_3. Pattern 5, taken at the relatively low resistivity point of ∼70% Nb, shows only two peaks and does not allow for unequivocal phase identification, therefore it is not useful in explaining the source of the lower resistivity.

To find a structural explanation for the discontinued and scattered results, a few other points, with similar Nb percentages of ∼20% and ∼70%, were measured. These points are located at the edges of the library, where the lowest resistivity was measured, and are labeled in Figure 6c as A, B, C, and D. The XRD patterns of these points are shown in Figure 6d. Points A and B have a similar composition to point 3

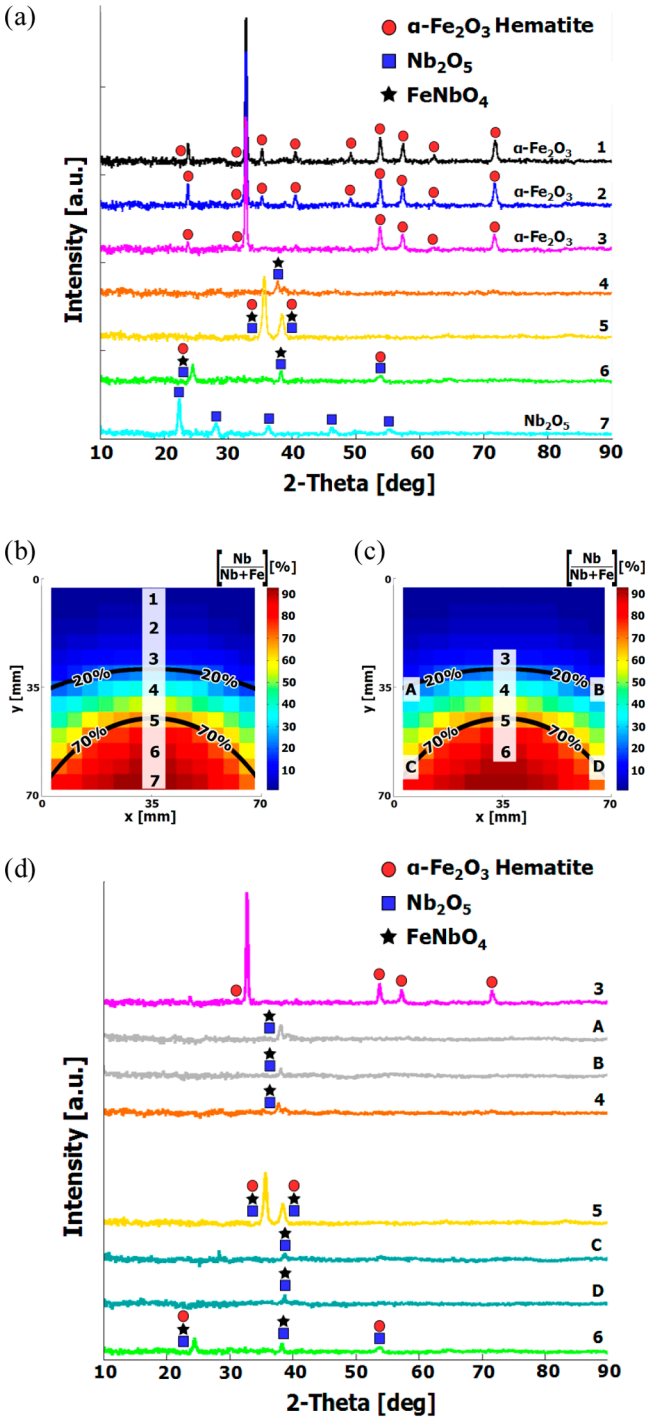

Figure 6. (a) XRD patterns taken along a vertical line in the center of the library. The patterns are labeled by their vertical position in the library (b): Patterns 1, 2, and 3 indicate that α-Fe_2O_3 is the only crystalline phase present in these parts of the library, pattern 7 indicates Nb_2O_5 is the only crystalline phase present at this point. Patterns 4, 5, and 6 are inconclusive, since the peaks correspond to several phases. Points with ∼20% and ∼70% Nb are indicated with black contours. (c) XRD patterns taken along two semicircular rings, each with the same composition, respectively (d): points 3, A, and B, each with ∼20% Nb atomic percentage, and point 4 is shown for comparison; points 5, C, and D, each with ∼70% Nb atomic percentage, and point 6 is shown for comparison. Despite the similar composition, in both rings there is a significant difference between points along the central vertical line and points at the edges, in both the level of crystallinity and the crystalline phases present.

DOI: 10.1021/co500094h
ACS Comb. Sci. 2015, 17, 209−216

(~20% Nb), however, their patterns are more similar to the pattern of point 4, which contains ~35% Nb. In the same way, points C and D share a similar composition to point 5 (~70% Nb) but their patterns are more similar to pattern 6, which contains ~85% Nb. Despite the similar composition, in both rings (~70% and ~20% Nb) there is a significant difference between points along the central vertical line and points at the edges, in both the level of crystallinity and the crystalline phases present. In other words, it is evident that points with similar chemical composition do not have the same crystalline structure. It is likely that the main cause for that is the lateral inhomogeneity of the PLD deposited films, as observed in the hierarchical clustering analysis described above.

The lateral inhomogeneity of the film can be also observed in the SEM images taken along the 20% Nb line, that are shown in Figure 7. A significant morphological dissimilarity between the

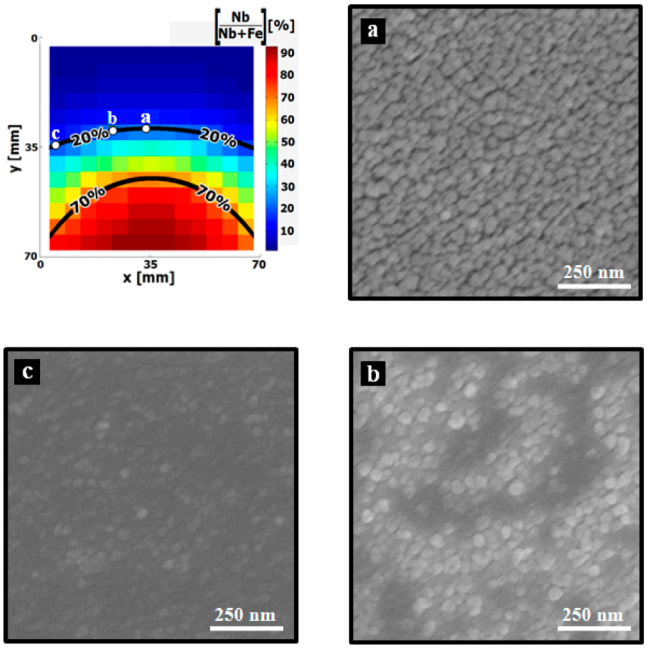

Figure 7. SEM images of the Fe−Nb−O layer at three different points with 20% Nb: (a) close to the center of the sample, along the central vertical line; (b) intermediate point between the center and the edge of the sample; (c) close to the edge of the sample. Images a and c show similar surface coverage. However, there is a major difference between them, as point a has bigger particles (~20−50 nm) than point c. The intermediate point b contains both large and small particles as a mixture that covers the surface. The top left figure shows the positions on the library where the SEM images were taken.

different points is observed. Point a, that is located close to the center of the sample, along the central vertical line, contains mainly particles sized 20−50 nm, that cover the surface almost uniformly. In contrast, point c, which is located close to the edge of the sample, contains much smaller particles (<5 nm). Point b, located in between points a and c, contains a mixture of both small and large particles.

As the chemical composition of these points is similar (~20% Nb), the different morphology might be the cause for the electrical resistivity variation, as seen in previous studies.[41] Following this interpretation it is either the smaller particle size or the amorphous material present in point c that induces the higher conductivity.[42] This approach cannot explain the results throughout the library and is therefore regarded as one of the outcomes of distance of deposition from the center of the Fe_2O_3 PLD plasma plume.

Besides the morphology, other factors that originate from the PLD lateral inhomogeneity might contribute to different physical properties of the layer. As discussed above, the lateral inhomogeneity causes structural changes, which in turn may affect the electrical conductivity. Other factors that can affect the electrical conductivity include the specific deposition conditions and the oxidation states of the metal cations in the film. Even though we were not yet able to resolve the exact nature of the low resistivity points, we showed that the lowest resistivity is achieved in the periphery of the library, in areas far from the center of the PLD plasma plume. These areas could not be explored while using the mask-based approach. By applying hierarchical clustering analysis on the Raman and UV−vis spectroscopy data, the importance of the distance from the center of the α-Fe_2O_3 PLD plasma plume was emphasized, since only the ~20% Nb points that were far from the center of the α-Fe_2O_3 PLD plasma plume displayed low resistivity. All the above leads us to conclude that despite the lateral inhomogeneity of the library, caused by the way the PLD deposition was performed without the use of masks, it is possible to study such a complex library. Moreover, the inhomogeneous deposition nature throughout the PLD-deposited library can be seen as an additional degree of freedom. Using hierarchical clustering analysis, the role of each of the parameters varying across the library is highlighted−the chemical composition, as well as the PLD deposition nature. Such an approach enables the investigation of large libraries deposited with PLD, without using masks and without the need to reduce the library's level of complexity.

CONCLUSIONS

We demonstrated a new approach to handle the lateral inhomogeneity in PLD-deposited films, using an Fe−Nb−O library as a model system. The library was measured using high-throughput scanners for electrical, structural, and optical properties. A notable decrease in the electrical resistivity (ρ) at ~20% Nb was achieved (measured at 47 and 267 °C), which is several orders of magnitude lower than the pure α-Fe_2O_3 resistivity. Utilizing hierarchical clustering analysis on the Raman and UV−vis spectroscopy data, we emphasized the effect of the distance from the center of the α-Fe_2O_3 PLD plasma plume on the material properties, showing that only the ~20% Nb points that were far from the center of the α-Fe_2O_3 PLD plasma plume displayed low resistivity. Using hierarchical clustering analysis, the role of each of the parameters, varying throughout the library was highlighted: the chemical composition, as well as the PLD deposition nature. We concluded that the inhomogeneous PLD deposition throughout the library can be seen as an additional degree of freedom, as long as proper analytical tools, such as hierarchical clustering analysis, are utilized.

ASSOCIATED CONTENT

Supporting Information

Thickness profiles of the Fe_2O_3 and the Nb_2O_5 reference samples, hierarchical clustering analysis dendrogram of the Raman data, hierarchical clustering analysis dendrogram of the UV−vis absorptance data, indirect bandgap map, direct bandgap map, and plots of both direct and indirect bandgaps as a function of composition. This material is available free of charge via the Internet at http://pubs.acs.org.

DOI: 10.1021/co500094h
ACS Comb. Sci. 2015, 17, 209−216

AUTHOR INFORMATION

Corresponding Author

*E-mail: Arie.Zaban@biu.ac.il.

Funding

This project has received funding from the Israeli National Nanotechnology Initiative (INNI, FTA project), and from the European Commission under the FP7 AllOxidePV project entitled "Novel Composite Oxides by Combinatorial Material Synthesis for Next Generation All-Oxide-Photovoltaics", Number 309018.

Notes

The authors declare no competing financial interest.

ACKNOWLEDGMENTS

We thank A. Gilad Kusne and Christian Long for providing the CombiView software, and Kevin J. Rietwyk for assisting in proofreading the manuscript.

REFERENCES

(1) Christen, H. M.; Silliman, S. D.; Harshavardhan, K. S. Epitaxial superlattices grown by a PLD-based continuous compositional-spread technique. *Appl. Surf. Sci.* **2002**, *189* (3−4), 216−221.

(2) Lowndes, D. H.; Geohegan, D. B.; Puretzky, A. A.; Norton, D. P.; Rouleau, C. M. Synthesis of novel thin-film materials by pulsed laser deposition . *Science* **1996**, *273* (5277), 898−903.

(3) Christen, H. M.; Eres, G. Recent advances in pulsed-laser deposition of complex oxides. *J. Phys.: Condens. Matter* **2008**, *20* (26), No. 264005.

(4) Maier, W. F.; Stöwe, K.; Sieg, S. Combinatorial and high-throughput materials science. *Angew. Chem., Int. Ed.* **2007**, *46* (32), 6016−6067.

(5) Hans, M. C.; Isao, O.; Christopher, M. R.; Gerald, E. J., Jr.; Alex, A. P.; David, B. G.; Douglas, H. L. A laser-deposition approach to compositional-spread discovery of materials on conventional sample sizes. *Meas. Sci. Technol.* **2005**, *16* (1), 21.

(6) Christen, H. M.; Rouleau, C. M.; Ohkubo, I.; Zhai, H. Y.; Lee, H. N.; Sathyamurthy, S.; Lowndes, D. H. An improved continuous compositional-spread technique based on pulsed-laser deposition and applicable to large substrate areas. *Rev. Sci. Instrum.* **2003**, *74* (9), 4058−4062.

(7) Ohkubo, I.; Christen, H. M.; Khalifah, P.; Sathyamurthy, S.; Zhai, H. Y.; Rouleau, C. M.; Mandrus, D. G.; Lowndes, D. H. Continuous composition-spread thin films of transition metal oxides by pulsed-laser deposition. *Appl. Surf. Sci.* **2004**, *223* (1−3), 35−38.

(8) Takeuchi, I. Combinatorial Pulsed Laser Deposition. In *Pulsed Laser Deposition of Thin Films*; Eason, R., Ed.; John Wiley & Sons, Inc.: New York, 2006; pages 161−175.

(9) Kukuruznyak, D. A.; Ahmet, P.; Yamamoto, A.; Ohuchi, F.; Chikyow, T. Combinatorial fabrication and characterization of ternary La_2O_3−Mn_2O_3−Co_3O_4 Composition Spreads. *Jpn. J. Appl. Phys.* **2005**, *44* (8R), 6164.

(10) Christen, H. M.; Silliman, S. D.; Harshavardhan, K. S. Continuous compositional-spread technique based on pulsed-laser deposition and applied to the growth of epitaxial films. *Rev. Sci. Instrum.* **2001**, *72* (6), 2673.

(11) Christen, H. M.; Ohkubo, I.; Rouleau, C. M.; JellisonJr, G. E.; Puretzky, A. A.; Geohegan, D. B.; Lowndes, D. H. A laser-deposition approach to compositional-spread discovery of materials on conventional sample sizes. *Meas. Sci. Technol.* **2005**, *16* (1), 21−31.

(12) Rühle, S.; Anderson, A. Y.; Barad, H.-N.; Kupfer, B.; Bouhadana, Y.; Rosh-Hodesh, E.; Zaban, A. All-oxide photovoltaics. *J. Phys. Chem. Lett.* **2012**, *3* (24), 3755−3764.

(13) Takeuchi, I.; Lauterbach, J.; Fasolka, M. Combinatorial materials synthesis. *Mater. Today* **2005**, *8* (10), 18−26.

(14) Khare, C.; Sliozberg, K.; Meyer, R.; Savan, A.; Schuhmann, W.; Ludwig, A. Layered WO_3/TiO_2 nanostructures with enhanced photocurrent densities. *Int. J. Hydrogen Energy* **2013**, *38* (36), 15954−15964.

(15) Cornell, R. M.; Schwertmann, U. *The Iron Oxides*, 2nd ed.; Wiley: New York, 2003.

(16) Walker, T. R. Formation of red beds in modern and ancient deserts. *Geol. Soc. Am. Bull.* **1967**, *78* (3), 353−368.

(17) Badia-Bou, L.; Mas-Marza, E.; Rodenas, P.; Barea, E. M.; Fabregat-Santiago, F.; Gimenez, S.; Peris, E.; Bisquert, J. Water oxidation at hematite photoelectrodes with an iridium-based catalyst. *J. Phys. Chem. C* **2013**, *117* (8), 3826−3833.

(18) Klahr, B.; Gimenez, S.; Fabregat-Santiago, F.; Bisquert, J.; Hamann, T. W. Electrochemical and photoelectrochemical investigation of water oxidation with hematite electrodes. *Energy Environ. Sci.* **2012**, *5* (6), 7626−7636.

(19) Sivula, K.; Le Formal, F.; Grätzel, M. Solar water splitting: Progress using hematite (α-Fe_2O_3) photoelectrodes. *ChemSusChem* **2011**, *4* (4), 432−449.

(20) Glasscock, J. A.; Barnes, P. R. F.; Plumb, I. C.; Bendavid, A.; Martin, P. J. Structural, optical and electrical properties of undoped polycrystalline hematite thin films produced using filtered arc deposition. *Thin Solid Films* **2008**, *516* (8), 1716−1724.

(21) Kennedy, J. H.; Frese, K. W. Photooxidation of water at α-Fe_2O_3 electrodes. *J. Electrochem. Soc.* **1978**, *125* (5), 709−714.

(22) Dare-Edwards, M. P.; Goodenough, J. B.; Hamnett, A.; Trevellick, P. R. Electrochemistry and photoelectrochemistry of iron(III) oxide. *J. Chem. Soc., Faraday Trans. 1* **1983**, *79* (9), 2027−2041.

(23) Cherepy, N. J.; Liston, D. B.; Lovejoy, J. A.; Deng, H.; Zhang, J. Z. Ultrafast studies of photoexcited electron dynamics in γ- and α-Fe_2O_3 semiconductor nanoparticles. *J. Phys. Chem. B* **1998**, *102* (5), 770−776.

(24) Joly, A. G.; Williams, J. R.; Chambers, S. A.; Xiong, G.; Hess, W. P.; Laman, D. M. Carrier dynamics in α-Fe_2O_3 (0001) thin films and single crystals probed by femtosecond transient absorption and reflectivity. *J. Appl. Phys.* **2006**, *99* (5), No. 053521.

(25) Bjoerksten, U.; Moser, J.; Graetzel, M. Photoelectrochemical studies on nanocrystalline hematite films. *Chem. Mater.* **1994**, *6* (6), 858−863.

(26) Wheeler, D. A.; Wang, G.; Ling, Y.; Li, Y.; Zhang, J. Z. Nanostructured hematite: Synthesis, characterization, charge carrier dynamics, and photoelectrochemical properties. *Energy Environ. Sci.* **2012**, *5* (5), 6682−6702.

(27) Warren, S. C.; Voïtchovsky, K.; Dotan, H.; Leroy, C. M.; Cornuz, M.; Stellacci, F.; Hébert, C.; Rothschild, A.; Grätzel, M. Identifying champion nanostructures for solar water-splitting. *Nat. Mater.* **2013**, *12*, 842−849.

(28) He, J.; Parkinson, B. A. Combinatorial Investigation of the Effects of the Incorporation of Ti, Si, and Al on the Performance of α-Fe_2O_3 Photoanodes. *ACS Comb. Sci.* **2011**, *13* (4), 399−404.

(29) Rajan, K. Combinatorial materials sciences: Experimental strategies for accelerated knowledge discovery. *Annu. Rev. Mater. Res.* **2008**, *38* (1), 299−322.

(30) Periasamy, P.; Berry, J. J.; Dameron, A. A.; Bergeson, J. D.; Ginley, D. S.; O'Hayre, R. P.; Parilla, P. A. Fabrication and characterization of MIM diodes based on Nb/Nb_2O_5 via a rapid screening technique. *Adv. Mater. (Weinheim, Ger.)* **2011**, *23* (27), 3080−3085.

(31) Shannon, R. Revised effective ionic radii and systematic studies of interatomic distances in halides and chalcogenides. *Acta Crystallogr., Sect. A* **1976**, *32* (5), 751−767.

(32) Anderson, A. Y.; Bouhadana, Y.; Barad, H.-N.; Kupfer, B.; Rosh-Hodesh, E.; Aviv, H.; Tischler, Y. R.; Rühle, S.; Zaban, A. Quantum efficiency and bandgap analysis for combinatorial photovoltaics: Sorting activity of Cu−O compounds in all-oxide device libraries. *ACS Comb. Sci.* **2014**, *16* (2), 53−65.

(33) Shimanovich, K.; Bouhadana, Y.; Keller, D. A.; Rühle, S.; Anderson, A. Y.; Zaban, A. Four-point probe electrical resistivity scanning system for large area conductivity and activation energy mapping. *Rev. Sci. Instrum.* **2014**, *85* (5), No. 055103.

DOI: 10.1021/co500094h
ACS Comb. Sci. 2015, 17, 209−216

(34) Thiess, W. *CODE: Thin Film Analysis and Design Software*, version 3.75; W. Theiss Hard- and Software: Aachen, Germany, 2012.
(35) O'Leary, S. K.; Johnson, S. R.; Lim, P. K. The relationship between the distribution of electronic states and the optical absorption spectrum of an amorphous semiconductor: An empirical analysis. *J. Appl. Phys.* **1997**, *82* (7), No. 3334.
(36) Kan, D.; Long, C. J.; Steinmetz, C.; Lofland, S. E.; Takeuchi, I. Combinatorial search of structural transitions: Systematic investigation of morphotropic phase boundaries in chemically substituted BiFeO3. *J. Mater. Res.* **2012**, *27* (21), 2691−2704.
(37) Long, C. J.; Hattrick-Simpers, J.; Murakami, M.; Srivastava, R. C.; Takeuchi, I.; Karen, V. L.; Li, X. Rapid structural mapping of ternary metallic alloy systems using the combinatorial approach and cluster analysis. *Rev. Sci. Instrum.* **2007**, *78* (7), No. 072217.
(38) Hastie, T.; Tibshirani, R.; Friedman, J. *The Elements of Statistical Learning*, 2nd ed.; Springer New York Inc.: New York, 2008.
(39) Yu, P. Y.; Cardona, M. *Fundamentals of Semiconductors*, 4th ed.; Springer: Berlin, 1996.
(40) Morin, F. J. Electrical properties of α-Fe_2O_3 and α-Fe_2O_3 containing titanium. *Phys. Rev.* **1951**, *83* (5), 1005−1010.
(41) Chopra, K. L. *Thin Film Phenomena*; McGraw-Hill: New York, 1979.
(42) Maissel, L. I.; Glang, R.; Budenstein, P. P. *Handbook of Thin Film Technology*; McGraw-Hill: New York, 1971.

DOI: 10.1021/co500094h
ACS Comb. Sci. 2015, 17, 209−216